Edge turbulence in different density regimes in Alcator C-Mod experiment

2011 Nucl. Fusion 51 053020

(http://iopscience.iop.org/0029-5515/51/5/053020)

IOP Publishing and International Atomic Energy Agency Nuclear Fusion
Nucl. Fusion **51** (2011) 053020 (9pp) doi:10.1088/0029-5515/51/5/053020

Edge turbulence in different density regimes in Alcator C-Mod experiment

M. Agostini[1], J.L. Terry[2], P. Scarin[1] and S.J. Zweben[3]

[1] Consorzio RFX, Associazione EURATOM-Enea sulla fusione, C.so Stati Uniti 4, I-35127, Padova, Italy
[2] Plasma Science and Fusion Center, Massachusetts Institute of Technology, 167 Albany Street, Cambridge, MA 02138, USA
[3] Princeton Plasma Physics Laboratory, Princeton, NJ, USA

E-mail: matteo.agostini@igi.cnr.it

Received 30 November 2010, accepted for publication 18 March 2011
Published 27 April 2011
Online at stacks.iop.org/NF/51/053020

Abstract
Plasma edge turbulence of Alcator C-Mod tokamak is studied with a fast camera in different density regimes. The statistical properties of the fluctuations, as well as the behaviour of the blobs, are characterized in plasma discharges at different normalized densities, studying the link between the edge turbulence and the Greenwald limit. It is shown that approaching the Greenwald density limit, the edge velocity field measured with the cross-correlation technique changes and the strong fluctuations, which for standard discharges develop mainly outside the separatrix, extend also in the radial region inside the last closed flux surface. At the same time, the blobs cover a larger radial region, suggesting a strong impact of the edge turbulence and transport on the Greenwald limit.

(Some figures in this article are in colour only in the electronic version)

1. Density limit and edge turbulence

The Greenwald scaling law describes the maximum plasma density n/n_G that can be reached both in tokamak and reversed field pinch (RFP) fusion experiments [1, 2], with the Greenwald density defined as

$$n_G = \frac{I_p}{\pi a^2} \, [10^{20}\,\mathrm{m}^{-3}] \tag{1}$$

where I_p is the plasma current in MA and a the minor radius.

Although the phenomenology of this limit is well described and seems to be related to changes in the plasma edge, the underlying physics is still not understood. In Alcator C-Mod there is some evidence that when the Greenwald density is approached there are important changes in the plasma edge transport: the perpendicular transport increases with respect to the parallel conductivity, and the zone of strong cross-field transport moves inside the separatrix into the main plasma; these measurements, based mainly on the signals collected by Langmuir probes, are reported in [3]. More recently, measurements made with the new gas puff imaging (GPI) system show a clear increase in the edge fluctuation power at $n/n_G > 0.3$–0.4, as described in [4]. In this paper, the characterization of the plasma edge of Alcator C-Mod experiment [5] is carried out in discharges at different normalized densities using the fast camera to measure the edge turbulence and blobs. The main aim of the paper is to study the link between the plasma edge (and particularly the edge fluctuations) and the density limit. In the first part of the paper the propagation velocity of the edge fluctuations in the plane perpendicular to the local magnetic field is measured. In the second part the behaviour of the edge blobs is studied as the density is increased with the conditional average (CA) technique applied to the images.

2. Experimental set-up

The edge region of Alcator C-Mod is studied here with the spectroscopic diagnostic called gas puff imaging (GPI) [6, 7]. It measures in the outer midplane the light emission of the neutral D_α (or He I) locally puffed into deuterium discharges. The fluctuations of the light emission I are proportional to the local electron temperature and density $I \propto n_e^\alpha T_e^\beta$ [8]. These fluctuations are measured with a Phantom 7.3 camera: it has 64×64 square pixels ($11.5\,\mu\mathrm{m} \times 11.5\,\mu\mathrm{m}$), and normally operates at 250 kHz frame rate acquiring 30 000 frames (120 ms during the flat top of the plasma discharge). The camera's view is focused in the edge region near the separatrix (whose position is known with an uncertainty of about 4 mm), to observe the light fluctuations in the perpendicular plane, i.e. the radial poloidal one. The D_α or He I cloud has a toroidal extent that can be estimated with the DEGAS-2

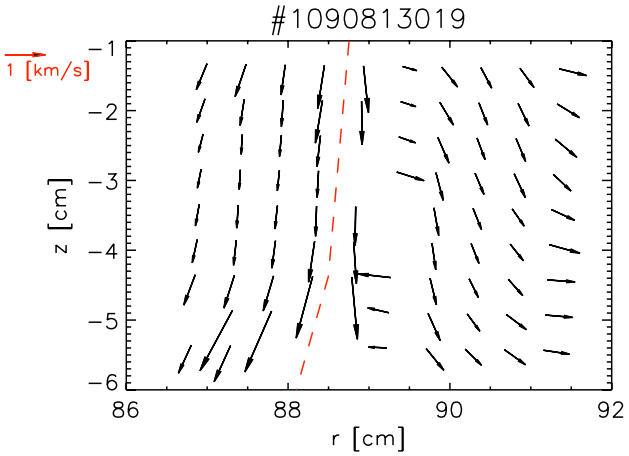

Figure 1. Velocity field of the edge fluctuations for a low density discharge ($n/n_G \approx 0.2$, $I_p = 1.1$ MA, $B_T = 5.4$ T). The vertical dashed line is the position of the separatrix. Downward propagation is in the ion diamagnetic drift direction in these discharges. The arrow on the top left of the figure has $[v_r, v_z] = [1, 0]$ km s^{-1} and is used as a reference.

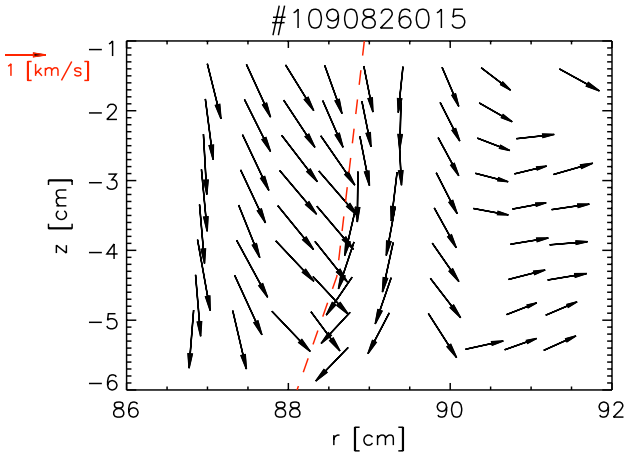

Figure 2. Velocity field of the edge fluctuations for a high density discharge ($n/n_G \approx 0.6$, $I_p = 0.8$ MA, $B_T = 5.4$ T). The vertical dashed line is the position of the separatrix. Downward propagation is in the ion diamagnetic drift direction. The arrow on the top left of the figure has $[v_r, v_z] = [1, 0]$ km s^{-1} and is used as a reference.

code [9, 10] of about 15 mm full width at half maximum at the outermost edge and about 50 mm at the separatrix location. This affects the radial resolution of the diagnostic since the views are integrating the turbulence fluctuations through the cloud; however, this effect is negligible since the camera view is aligned with the local magnetic field, and the structures are field-aligned as first approximation. The discharges analysed in this paper are in lower single null configuration, ohmically heated, with plasma current $I_p = 0.4$–1.2 MA and the toroidal magnetic field in the range 2.3–5.4 T; the normalized density is varied $n/n_G = 0.2$–0.6 to characterize the turbulence in different density regimes. In this Ohmic current scan the safety factor $q(a)$ does not vary.

In order to have data also at higher normalized density, some plasma discharges in limiter configuration have been analysed, with $I_p = 0.8$ MA and $B_T = 5.4$ T. In these discharges a value of $n/n_G = 0.8$ is reached. In the high density discharges, helium is puffed (instead of deuterium) in deuterium plasma, in order to increase the contrast between the GPI light and the background light. In this way, similar contrast is obtained for low and high density plasma.

3. Edge turbulence at low and high plasma density

A first look at the behaviour of the edge region at different plasma densities can be studied measuring the velocity fields of the edge fluctuations. To do this, the camera field of view of 64 × 64 pixels is divided into smaller square regions of 10 × 10 pixels, and a 10 ms time interval is considered, during the flat-top of the plasma current; the cross-correlation between the pixels in each square is evaluated, and from the time delay of the maximum of the correlation it is possible to compute the 2D velocity [11]. This is a measurement of the propagation velocity of all the edge fluctuations, not only the coherent blobs, since the whole signal is considered. The results are shown in figure 1 for low density ($n/n_G = 0.2$) and figure 2 for higher density ($n/n_G = 0.6$) discharges. These are two typical discharges representative of the average behaviour of the two density regimes; however, the details of the 2D flow can change when analysing different plasma shots. For both the density regimes two distinct regions can be recovered, divided radially by the separatrix. When $n/n_G = 0.2$ (figure 1) inside the separatrix the velocity of the edge fluctuations is mainly poloidal, in the downward direction, with values of about -500 m s^{-1}. This is in the ion diamagnetic drift direction. Near the separatrix it is difficult to calculate the velocity, since the cross-correlation between the different pixels is not sufficiently high (<0.2) and this can explain the unclear behaviour of the velocity field in the range 88.5–89.5 cm for the low density discharge. It is not completely clear why inside the separatrix the velocity field inferred by the cross-correlation using the camera does not agree with electrostatic probe measurements for similar discharges (in these plasma shots the Langmuir probes were not available) [12]. Usually the electric field measured by the Langmuir probes shows an inversion across the separatrix, with the consequent inversion of the $\boldsymbol{E} \times \boldsymbol{B}$ velocity, which results in turbulence propagation along the electron diamagnetic drift. Here we can only suggest two possible causes, that should be investigated in the future: (1) the cross-correlation technique is mostly sensitive to the large amplitude fluctuations and to large blobs, differently from the probes, so the two measurements are referred to two different kinds of fluctuations; (2) inside the separatrix the fluctuations do not move only with the $\boldsymbol{E} \times \boldsymbol{B}$ flow. However, in [4], fluctuations inside the separatrix measured with the GPI fast diode diagnostic are seen to propagate in both the poloidal directions, when analysed using spatial and temporal Fourier transforms. The analysis often show that much of the lower frequency fluctuation power propagates in the ion diamagnetic drift direction, in agreement with the camera results.

Outside the separatrix the fluctuations propagate both in the poloidal and radial directions (outwards), with the radial component increasing with the distance from the separatrix. These results and values of the propagation velocities are in agreement with what have already been described in [13]. In the high density discharges (figure 2) the velocity field is

quite different: a strong radial component appears, both inside and outside the separatrix; outside the separatrix the velocity is almost entirely radial. These simple differences between high and low density plasmas suggest (if the transport in the SOL is not purely diffusive) an increase in the radial transport due to edge fluctuations by increasing n/n_G. In [3] it is shown that approaching the density limit in Alcator C-Mod, the perpendicular transport across the separatrix becomes larger with respect to the parallel heat losses to the divertor plates. The results of the velocity field measured here with the fast camera are qualitatively consistent with those observations.

It is also important to notice in figure 2 that in the most external region ($r > 90$ cm) the far SOL fluctuations can have a positive poloidal velocity (upwards, in the electron diamagnetic direction). This velocity inversion can be due to an inversion of the radial electric field in the SOL at high density, although a direct measurement of E_r in these discharges is not available. A similar phenomenology of the inversion of the edge flow at high n/n_G plasma shots, probably related to an inversion of the radial electric field, has been observed also in the RFX-mod RFP experiment [14–16].

In RFX-mod, when the density increases, there is a local inversion of the edge flow, so that two spatial regions can be distinguished, with opposite velocities. The edge flow transports the electrons in opposite directions, up to the point where this velocity is zero: here there is a local accumulation of density, with a subsequent decrease of temperature, increase in resistivity and the soft landing of the plasma current. It is interesting to note that, despite the different magnetic configurations, the RFP and tokamak exhibit the same density limit, namely n_G, and approaching this density, there are some similar phenomenologies in the behaviour of the plasma edge. This could be a hint at the existence of common physical mechanisms leading to the density limit in plasma fusion devices.

To see in a better way the dependence of the edge velocities with n/n_G, in figure 3 v_θ and v_r evaluated about 25 mm outside the separatrix are plotted as a function of the normalized density. The polodial velocity does not have a linear dependence with the normalized density. The important result of this plot is that only at higher density can v_θ assume positive values, i.e. along the electron diamagnetic drift direction. At low density, the far SOL propagation is always in the ion diamagnetic drift direction. Instead v_r shows a strong dependence with n/n_G. In particular, what happens in the poloidal velocity is clearer in figure 4, where the time evolution of v_θ for two different radial positions and for two different normalized densities is shown. At $n/n_G = 0.2$ the poloidal velocity varies in time but it is always negative (i.e. along the ion diamagnetic drift direction); at higher normalized density, the propagation velocity of the fluctuations changes sign during the discharge, so it can assume both positive and negative values. Thus, if an average velocity is evaluated, at low density it assumes a negative value, and at higher density it can assume negative or positive value.

This inversion in the poloidal velocity appears when the normalized density is greater than 0.3–0.4. Also in RFX-mod the inversion of the edge velocity field and changes in the edge turbulence are observed for the same value of n/n_G [16, 17]. A sort of 'transition' in the behaviour of edge turbulence

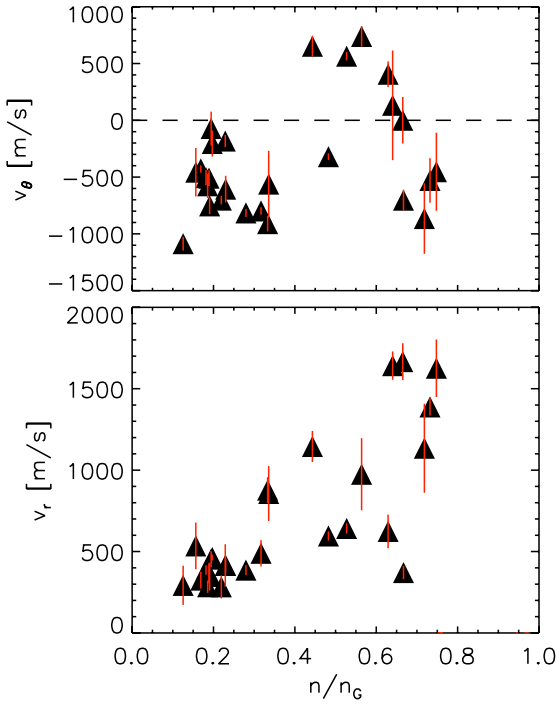

Figure 3. Up: poloidal velocity of the edge fluctuations at $\rho = 25$ mm as a function of the density normalized to the Greenwald one (negative velocity means in the ion diamagnetic drift direction). Bottom: same scaling for the radial velocity of the fluctuations, evaluated at the same radial position (positive velocity means outward propagation). The points with $n/n_G > 0.6$ are in the limiter configuration.

for the same range of normalized density is observed also in MAST [18].

The radial velocity increases with increasing normalized density, and its direction is always outwards. This result suggests that (1) increasing n/n_G changes the SOL turbulence properties; (2) at high normalized density the radial transport due to edge fluctuations may increase; (3) the edge could have a strong impact on the physics that cause the density limit in tokamak devices. This last sentence is valid since there is considerably experimental evidence from different fusion devices that the edge fluctuations and blobs are responsible for the most of the outward particle transport (see, for example, [19, 20] and references cited there for a review on this topic).

Beyond the velocity field of the fluctuations, it is interesting also to measure the radial and poloidal velocity of the blobs in this velocity field, comparing the behaviour at low and high density. In the time series of the camera pixels, the presence of an intermittent burst is detected with the *local intermittency measure* (LIM) method described in [21, 22]. This iterative method allows the signal to be divided into two parts: one with a Gaussian probability distribution function (PDF) and the second which is responsible for the strong positive tail of the PDF characteristic of the intermittent turbulent signals. In fact, the presence of coherent structures (blobs) in the edge plasma is normally observed in the time series signals as strong bursts emerging from the background. Once an edge burst is detected with the LIM in one pixel, a time interval of 0.1 ms (25 time samples) around it is selected, and the cross-correlation is evaluated between all the nearest

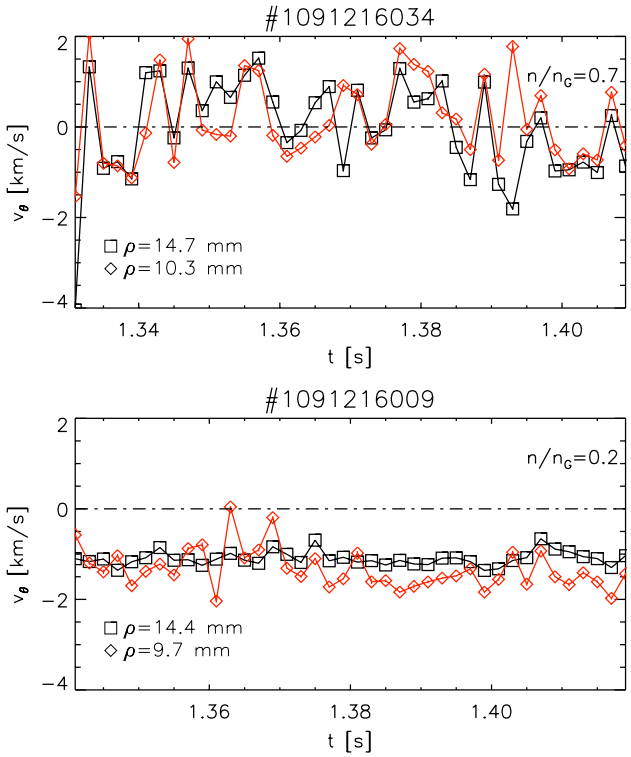

Figure 4. Time evolution of the poloidal velocity of the SOL fluctuations evaluated with the cross-correlation technique at two different radial positions with respect to the separatrix (ρ) for discharges with two different normalized density. Top: high density discharge, where v_θ changes sign during time; bottom: low density discharge, where v_θ is negative for all the times considered.

7 + 7 poloidal and radial pixels. In this way, inside this small time and space window, only a single blob is present. From the cross-correlation it is possible to estimate v_r and v_θ of the blobs. In figure 5 the result of this analysis is shown: on the left for low density ($n/n_G = 0.2$), on the right for high density discharge ($n/n_G = 0.6$), for a radial position about 20 mm outside the separatrix. In the first two panels, the radial velocity of the blobs as a function of their poloidal one shows that they have a distribution of velocities: they can move both in the ion and electron diamagnetic drift directions (negative or positive v_θ), both inwards or outwards. Moreover, a clear relation between the two components of the velocity is not observed. In the two bottom panels, the PDFs of the velocities show a strong difference between the low (left) and high (right) plasma density. The distribution of v_r (red) in the two regimes is centred for positive (outward) values, like the average velocity of the fluctuations described in figures 1 and 2. However, there are blobs that move also from the SOL to the separatrix, going inwards. The greatest difference between low and high density regimes is in the distribution of the poloidal velocity of the blobs. At $n/n_G = 0.2$, the PDF of the blob poloidal velocity is centred in the ion diamagnetic drift direction (negative values). At $n/n_G = 0.6$ two peaks are present in the PDF, one for positive and one for negative v_θ, and the dominant one is the positive one: in the SOL, blobs move in both directions, most of them in the electron diamagnetic drift direction. For low density plasma similar PDF of the velocity of blobs is reported in [23, 24]. It is interesting to note that also in NSTX [25] and Caltech [26] experiments, blobs are seen to move in all directions, inwards and outwards, along the ion and electron drift directions, even if a mean flow is present.

Once these differences in the edge velocity field are observed, a deeper view of the behaviour of the edge fluctuations in different density regimes can be obtained from the spatial cross-correlation analysis. The whole camera field of view is divided into 6 × 6 square regions, a 10 ms time interval is considered, and the cross-correlation of the central pixel $p_c(t)$ with all the others $p_m(t)$ as a function of the time-lag (τ_l) is evaluated $C_{c,m}(\tau_l)$. In figure 6 the maximum of this correlation is shown, for the discharge with $n/n_G \approx 0.2$. This type of plot explains what is the spatial correlation of the fluctuations. In figure 6, at low density, outside the separatrix the correlation between adjacent pixels extends for more than 10 mm both in the radial and poloidal directions; it becomes very low inside the separatrix, with a sort of 'transition' across it (the two lowest and most external squares show a low correlation caused by noisy signal of the camera in that region). Inside the separatrix the fluctuations are uncorrelated; outside the correlation increases both in the value and in spatial extensions. The same plot is reported in figure 7, but for $n/n_G \approx 0.6$. Here the correlation remains high (>0.5) also inside the separatrix: the spatially correlated fluctuations, which for low density discharges characterize mainly the SOL, at high density extend also inside. Similarly, in [3, 27] it is reported that increasing the normalized plasma density, the autocorrelation times and the normalized ion saturation current fluctuation amplitudes measured with electrostatic probes become larger across the entire SOL. The spatial cross-correlation analysis of the camera data presented here shows that the region of strong turbulence with spatially correlated fluctuations, that for low density is confined outside the separatrix, extends radially entering the separatrix when n/n_G increases.

The next step in clarifying the behaviour of SOL turbulence at different density regimes is to study the SOL blobs. In the analysis described (velocity of the fluctuations and correlations), all frequency and amplitude ranges in the emission fluctuations have been considered, thus both fluctuations due to blobs and those not associated with coherent structures. In the next section the attention is focused on the blobs, since they affect strongly all the SOL plasma and they are considered to be the cause of most of the particle transport in the far SOL.

4. 2D conditional average

The study of the edge blobs is performed here with the CA technique [28, 29] applied to the camera data, in order to obtain information about the 'average blob' in different plasma conditions. An alternative method to make similar studies could be the detection and tracking of the single coherent structure and then make a statistical analysis. This detection and tracking method was applied for the analysis of the NSTX edge turbulence data measured with fast camera [30] and for the study of the turbulence of basic plasma measured with electrostatic probes [31, 32].

The CA technique consists in finding all the time instants when a blob is detected by the camera, and then making a

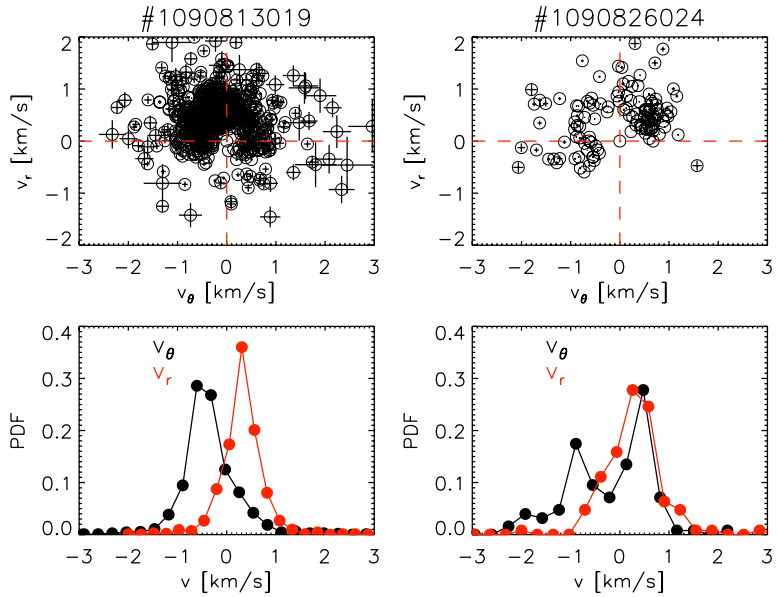

Figure 5. Radial velocity of the edge coherent structures as a function of the poloidal one for low (left) and high (right) density discharges $n/n_G = 0.2$ and $n/n_G = 0.6$, respectively, evaluated 2 cm outside the separatrix. In the bottom, the PDF for poloidal (black) and radial (red) velocities. Positive radial velocity means outwards, negative poloidal velocity means in the ion diamagnetic drift direction.The two discharges are in lower single null configuration.

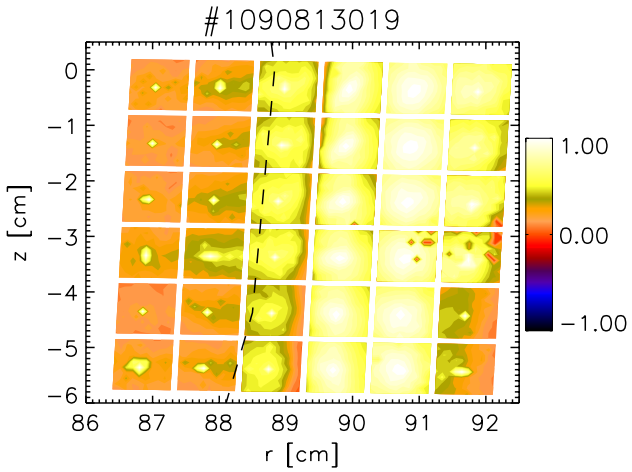

Figure 6. 2D cross-correlation of the camera data for a low density discharge ($n/n_G = 0.2$). The vertical black line is the separatrix.

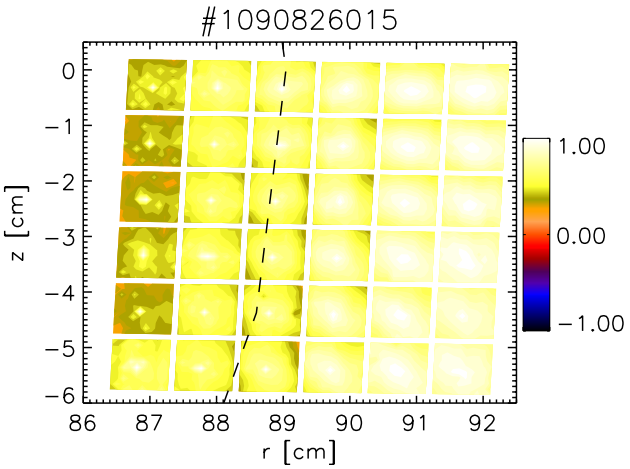

Figure 7. 2D cross-correlation of the camera data for a high density discharge ($n/n_G = 0.6$). The vertical black line is the separatrix.

spatial average to determine the mean (i.e. time-averaged) blob. In order to detect the time instant when a intermittent structure is present in the camera, 18 time series signals are built, summing together the emission of 3 poloidal $\times$ 3 radial pixels; this is done to have a better signal to noise ratio. These 18 signals are *probes*. In figure 8 the locations of these 18 probes (made by summing 3 $\times$ 3 pixel signals) are shown as squares, superimposed on one normalized frame from the camera time sequence. In the same figure the black line is the separatrix; also visible in the outermost radial region is the presence of one blob, seen as a region of higher light emission. In the time signal of the probes, the presence of an intermittent burst is detected with the LIM, described in the previous session. For all the 18 probes it is possible to find the time instants t^* when an intermittent burst is detected, and they are used as reference time for the computation of the CA.

Letting $I(t, r, z)$ be the time-varying signal measured by the pixel viewing the small region centred at (r, z), the normalized signal from that region is defined as

$$S(t, r, z) = \frac{I(t, r, z) - \langle I(t, r, z)\rangle}{\mathrm{rms}(I(t, r, z))} \tag{2}$$

where the time average and the standard deviation are evaluated for every (r, z) pixel. Then, for each 'probe' region, the 2D CA signal $\mathrm{CA}(\tau, r, z)$ can be evaluated:

$$\mathrm{CA}(\tau, r, z) = \sum_{n=t^*} S(n - \tau, r, z) \tag{3}$$

where τ is the time relative to the instant t^* when the burst is detected in one of the probes. The result is a sequence of 2D frames at different τ for each of the 18 different probe locations.

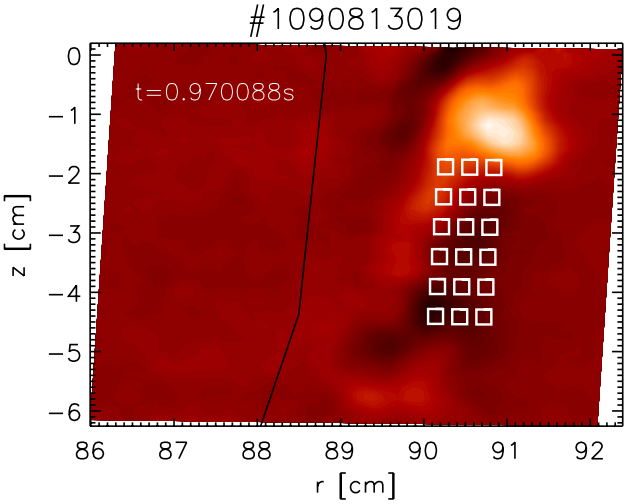

Figure 8. Example of one camera frame normalized to the RMS, with the separatrix (black line). The 3 radial × 6 poloidal squares represent the 18 ensemble of pixels ('probes') used for the CA analysis.

Ideally no differences are expected using reference probes with different poloidal positions and the same radial one, since the poloidal region covered by the camera is small and the properties of the turbulence have no poloidal dependence on this spatial scale. Then, to extract the coherent average structure from $\mathrm{CA}(\tau, r, z)$, all pixels whose conditionally averaged signal exceeds a threshold are considered to be a blob. Here one single threshold for all the time τ is used, and it is two standard deviations of the pixel signals. In this way, for every τ, *if* there are consecutive pixels that exceed the threshold, they are considered as part of a blob. The result of this detection and extraction of the average blob is summarized in figure 9. There is shown the time (τ) evolution of the conditionally averaged blob after being detected by one of the 18 probes. The time between frames is 8 μs and the average motion of the spreading structures is shown; the black dot is the centre of mass of the blob. Using these results, it is now possible to measure the area of the conditionally averaged blobs, how they evolve in time, and the radial position where they are born. In figure 10 the results of the CA analysis are shown for one shot as an example. In figure10(b) the area of the average blob as a function of the radial position during its motion is shown. The three different colours refer to the three different radial positions of the probes used as reference signal to detect the intermittent bursts (see figure 8, white squares). The result (area versus radial position) does not depend on the reference probe, since all the points are well superimposed on each other. The average blobs are seen to born at about $r = 90$ cm, between the two red vertical lines, since for smaller radius there are no pixels of the CA that exceed the selected threshold. Blobs that emerge radially at $r = 90$ cm evolve moving outwards increasing their dimension (area), reaching their maximum extension at about $r = 91$ cm. The subsequent decrease in the area is not real, since they begin to leave the field of view of the camera and their area is underestimated. In figure 10(a) these results are compared with the radial dependence of the autocorrelation time τ_a of the fluctuations of the camera pixels. Here τ_a is defined as twice the time when the autocorrelation assumes the value 0.5. For $r < 90$ cm, where no blobs are detected with the CA analysis, the autocorrelation time is small, about 10–15 μs; instead, for $r > 90$ cm, τ_a begins to increase up to 30 μs (similar values of the autocorrelation are reported also in [10]).

Summarizing, in the radial region near the separatrix (shadowed region in figure 10), the autocorrelation time of the edge fluctuations is small and no blobs are detected. This is also the region where the strong gradient of electron density and temperature develops [3]. Turbulence and blobs are well established outside the separatrix, where the autocorrelation time increases and coherent structures are detected, and where the electron profiles are quite flat. A similar relation between radial profiles and edge turbulence was observed also in the NSTX experiment [33, 34].

This CA analysis was performed for plasma discharges with different normalized density n/n_G. In particular, the radial position with respect to the separatrix where the average blobs are 'born' ρ_{birth} is measured as a function of n/n_G, and the result is reported in figure 11. Using the signal $\mathrm{CA}(\tau, r, z)$, the first frame when the average blob is detected can be identified, and it is considered as the time when it is born; the position of its centre of mass is defined as ρ_{birth}. At low density, namely $n/n_G < 0.3$–0.4, the coherent structures are born between 15 to 20 mm outside the separatrix, similarly to what is seen in figure 10. Increasing the normalized density, ρ_{birth} moves more inside, from the scrape-off layer towards the separatrix. With this analysis it is possible to give a numerical estimate of the birth region of the blobs for low and high plasma densities, which was only qualitatively shown and discussed in [35]. So increasing the normalized density, there is a strong change in the behaviour of the edge turbulence: the region of 'blobs birth' moves from the SOL to the separatrix, and the high spatial correlation of the light emission fluctuations (which indicates the presence of correlated turbulence and structures) extends radially, covering the whole SOL and part of the region inside the separatrix.

A complementary analysis (only for low density discharges) in which a link between the radial region where the blobs are born and the statistical properties of the edge fluctuations is studied can be found in [36].

It is important to recall that this analysis depends on the *definition of what a blob is*: here a blob is detected with the CA technique when there are adjacent pixels that exceed two standard deviations, but this is not the only possible choice. Since the definition of blob is the same for all the analysed discharges (both low and high density) it is possible to compare ρ_{birth} between plasma at different normalized densities; if the definition of blob is changed, the value of ρ_{birth} could change, but the relative difference between low and high n/n_G should remain. At the same time, the result that no blobs are detected inside the separatrix with this method could be partially due to the lower contrast of the GPI light in that region (near and inside the separatrix the neutral density of the puffed gas drops). However, the result reported in figure 11 (blobs are detected and are born nearer the separatrix at high n/n_G than lower density plasma) is in agreement with the cross-correlation analysis (see figures 6 and 7) and with the results shown for electrostatic probes in [3, 27]: in those papers it is reported that the autocorrelation time of floating potential and the ion saturation current fluctuations amplitude extend inside the LCFS only for high density discharges.

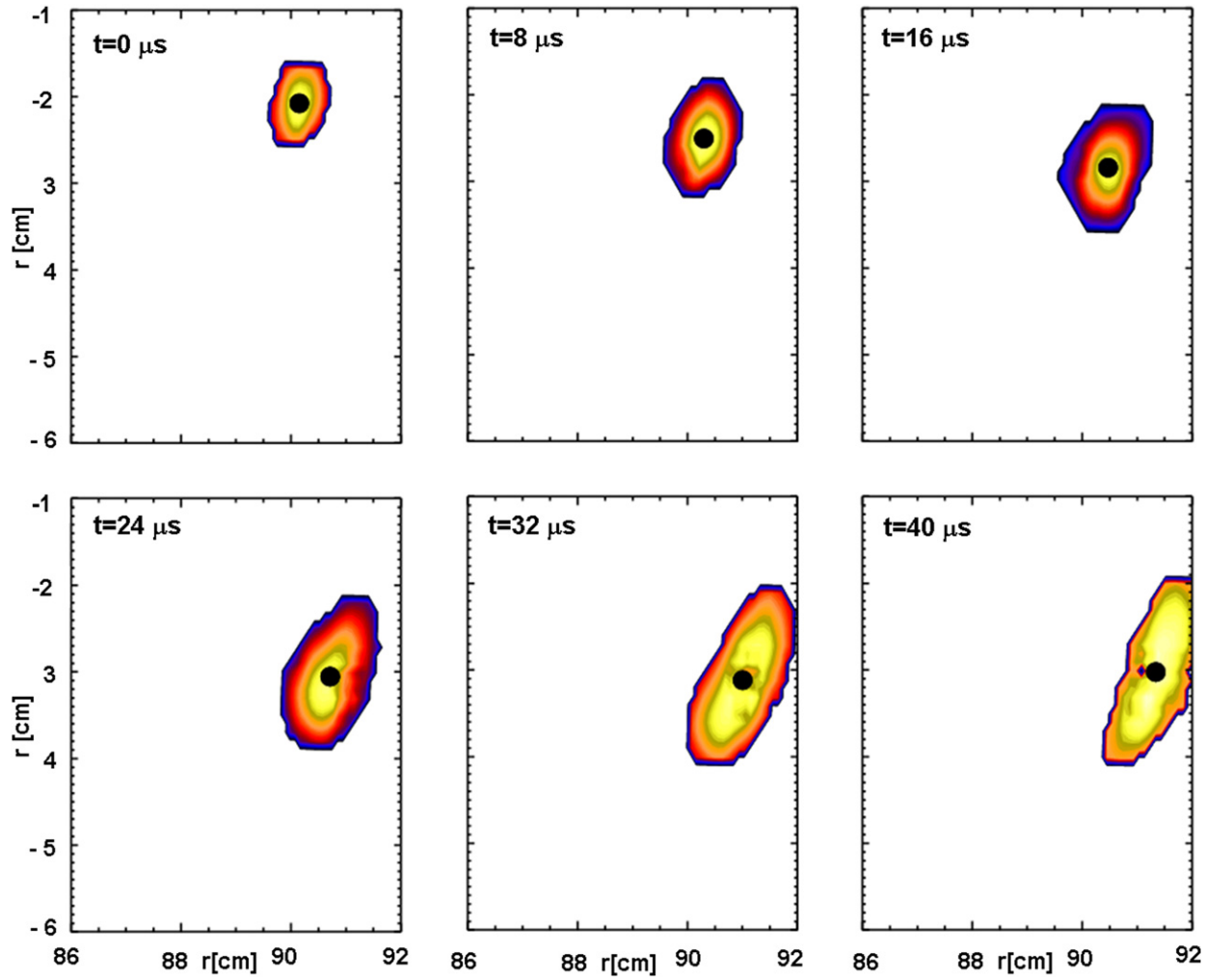

Figure 9. Result of the extraction of the average blob detected with the conditional average technique. The 6 frames shows the time evolution of the average blob, with its typical motion in the radial–poloidal plane. The black dot is the position of the centre of mass of the structure. The temporal resolution of the six images shown is 8 μs.

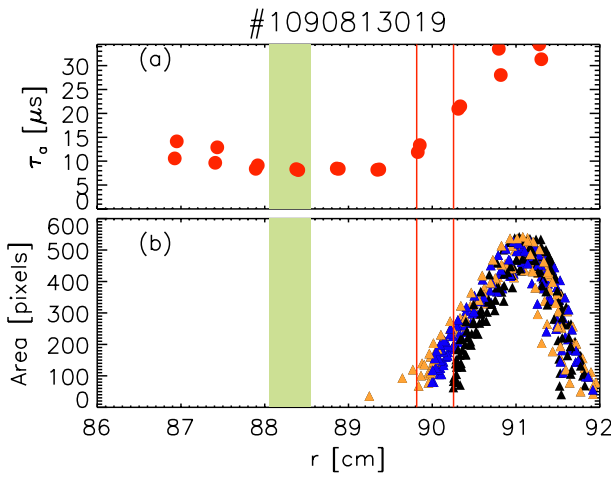

Figure 10. Autocorrelation time of the edge fluctuations (*a*) and area of the average blob (*b*) as a function of the radius. In (*b*), the three different colours refer to the three different radial positions of the probes used as reference signals for the conditional average. The shadowed region is the average position of the separatrix; the region enclosed by the two vertical red lines is where the average blobs are born.

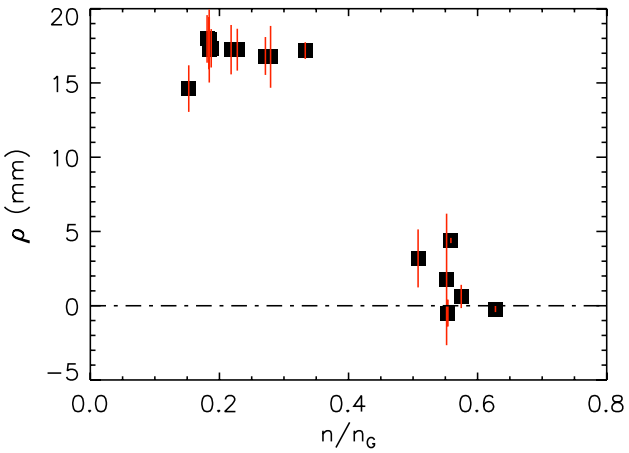

Figure 11. Radial position (with respect to the separatrix) where the average blobs are 'born' (see text) as a function of the density normalized to the Greenwald one. All the points refer to lower single null plasma discharges.

5. Conclusions

In this paper the behaviour of the edge fluctuations and turbulence of the Alcator C-Mod tokamak for different normalized densities have been characterized, in order to study the properties of the plasma edge and SOL as a function of plasma density, with an eye towards the role that the turbulence may play in the physics of the empirical density limit. It is shown that the properties of the edge turbulence change with increasing plasma density. The poloidal velocity of the edge fluctuations v_θ measured outside the separatrix for $n/n_G > 0.3$ can reverse its direction. For low density the poloidal phase velocity as measured using the time-delay cross-correlation analysis is in the ion-diamagnetic drift direction. At higher densities ($n/n_G > 0.3$–0.4) the fluctuation phase velocities in the most external region are observed to propagate in both the ion and electron diamagnetic drift directions. If the velocity of the edge fluctuations is mainly the $\boldsymbol{E} \times \boldsymbol{B}$ one, this should mean a change in the sign of E_r that occurs at higher density in the far SOL. This behaviour of the edge velocity is reflected also by measuring the velocity of individual blobs (figure 5).

A similar phenomenology of perpendicular flow inversion is observed in RFX-mod RFP device [14–16]. A change in the radial profile of E_r with n/n_G is predicted also in edge simulation as reported in [37]: by increasing the density, the E_r shear layer is destroyed, even if no changes in the sign of the electric field are foreseen. If E_r is modified by increasing the normalized density, then this phenomenon could affect the radial region where the blobs are born, as shown in [38, 39]

Looking at the radial velocity of the SOL fluctuations using the cross-correlation technique, it shows a strong scaling with n/n_G: v_r increases with the normalized density, from about 0.5 km s^{-1} at $n/n_G \approx 0.2$ to 1.5 km s^{-1} for $n/n_G \approx 0.8$ (the dominant direction is always outward). Since the fluctuations are responsible for the greatest part of the particle transport in the SOL, this result means that the convective perpendicular transport carried by turbulence increases at higher density. Together with the increase in the outward velocity, the edge region dominated by the turbulence extends more inside, towards the separatrix, and this is visible from the cross-correlation analysis of figures 1 and 2. At low density, most of the fluctuations are in the far SOL; at the same time, the blobs are 'born' about $\rho = 20$ mm outside the separatrix, and both the spatial and temporal correlations are high only for $\rho > 0$. For $n/n_G > 0.3$–0.4 the blobs are born near or inside the separatrix, and so the radial region dominated by structures and strong correlated fluctuations moves also at $\rho < 0$. All these observations suggest that the perpendicular transport due to edge and SOL turbulence is involved with the empirical density limit, though the causal relationships are still unclear.

Acknowledgments

M. Agostini thanks all the Alcator C-Mod team and in particular Istvan Cziegler for the constructive discussions and for the indispensable support received during the visits at MIT, and Dr Daren Stotler of PPPL for the discussion about the behaviour of the GPI neutral cloud in the plasma.

This work was supported by the US Department of Energy Cooperative Agreement No. DE-FC02-99ER54512 and by the European Communities under the Contract of Association between EURATOM and ENEA. The views and opinions expressed herein do not necessarily reflect those of the European Commission.

References

[1] Greenwald M. *et al* 1988 *Nucl. Fusion* **28** 2199
[2] Greenwald M. 2002 *Plasma Phys. Control. Fusion* **44** R27
[3] LaBombard B., Boivin R.L., Greenwald M., Hughes J., Lipschultz B., Mossessian D., Pitcher C.S., Terry J.L., Zweben S.J. and Alcator Group 2001 *Phys. Plasmas* **8** 2107
[4] Cziegler I., Terry J.L., Hughes J.W. and LaBombard B. 2010 *Phys. Plasmas* **17** 056120
[5] Hutchinson I.H. *et al* 1994 *Phys. Plasmas* **1** 1511
[6] Zweben S.J. *et al* 2002 *Phys. Plasmas* **9** 1981
[7] Terry J.L. *et al* 2003 *Phys. Plasmas* **10** 1739
[8] Stotler D.P., D'Ippolito D.A., LeBlanc B., Maqueda R.J., Myra J.R., Sabbagh A. and Zweben S.J. 2004 *Contrib. Plasma Phys.* **44** 294
[9] Stotler D.P., Boedo J., LeBlanc B., Maqueda R.J. and Zweben S.J. 2007 *J. Nucl. Mater* **363–365** 686
[10] Zweben S.J., Scott B.D., Terry J.L., LaBombard B., Hughes J.W. and Stotler D.P. 2009 *Phys. Plasmas* **16** 082505
[11] Serianni G., Agostini M., Cavazzana R. and Scarin P. 2007 *Plasma Phys. Control. Fusion* **49** 2075
[12] LaBombard B., Gangadhara S., Lipschultz B. and Pitcher C.S. 2003 *J. Nucl. Mater* **313–316** 995
[13] Terry J.L., Zweben S.J., Grulke O., Greenwald M.J. and LaBombard B. 2005 *J. Nucl. Mater* **337–339** 322
[14] Puiatti M.E. *et al* 2009 *Phys. Plasmas* **16** 012505
[15] Puiatti M.E. *et al* 2009 *Nucl. Fusion* **49** 045012
[16] Spizzo G. *et al* 2010 *Plasma Phys. Control. Fusion* **52** 095011
[17] Scarin P., Agostini M., Cavazzana R., Sattin F., Serianni G. and Vianello N. 2007 *J. Nucl. Mater* **363–365** 669
[18] Antar G.Y., Counsell G. and Ahn J.W. 2005 *Phys. Plasmas* **12** 082503
[19] Zweben S.J., Boedo J.A., Grulke O., Hidalgo C., LaBombard B., Maqueda R.J., Scarin P. and Terry J.L. 2007 *Plasma Phys. Control. Fusion* **49** S1
[20] Boedo J.A. 2009 *J. Nucl. Mater* **390–391** 29
[21] Onorato M., Camussi R. and Iuso R. 2000 *Phys. Rev.* E **61** 1447
[22] Antoni V., Carbone V., Martines E., Regnoli G., Serianni G., Vianello N. and Veltri P. 2001 *Europhys. Lett.* **54** 51
[23] Zweben S.J. *et al* 2011 Estimate of convective radial transport due to SOL turbulence as measured by GPI in Alcator C-Mod PSI paper, P3-20 *J. Nucl. Mater.* at press
[24] Grulke O., Terry J.L., LaBombard B. and Zweben S.J. 2006 *Phys. Plasmas* **13** 012306
[25] Zweben S.J. *et al* 2004 *Nucl. Fusion* **44** 134
[26] Zweben S.J. 1985 *Phys. Fluids* **28** 974
[27] LaBombard B., Greenwald M., Boivin R.L., Carreras B.A., Hughes J.W., Lipschultz B., Mossessian D., Pitcher C.S., Terry J.L., Zweben S.J. and Alcator C-Mod Team 2002 Density limit and cross-field edge transport scaling in Alcator C-Mod *Proceeding 19th Int. Conf. on Fusion Energy 2002 (Lyon, France, 2002)* (Vienna: IAEA) CD-ROM file EX/D2-1 and http://www.iaea.org/programmes/ripc/physics/fec2002/html/node120.htm
[28] Grulke O., Klinger T., Endler M., Piel A. and the W7-AS Team 2001 *Phys. Plasmas* **8** 5171
[29] Teliban I., Block D., Piel A. and Greiner F. 2007 *Plasma Phys. Control. Fusion* **49** 485
[30] Love N.S. and Kamathm C. 2007 *Proc. SPIE* **6696** 66960D

[31] Müller S.H. 2006 Turbulence in basic toroidal plasmas *PhD Thesis* http://crpp.epfl.ch/%7Etorpex/
[32] Müller S.H., Theiler C.H., Fasoli A., Furno I., Labit B., Tynan G.R., Xu M., Yan Z. and Yu J.H. 2009 *Plasma Phys. Control. Fusion* **51** 055020
[33] Myra J.R., D'Ippolito D.A., Stotler D.P., Zweben S.J., LeBlanc B.P., Menard J.E., Maqueda R.J. and Boedo J. 2006 *Phys. Plasmas* **13** 092509
[34] Agostini M., Zweben S.J., Cavazzana R., Scarin P., Serianni G., Maqueda R.J. and Stotler D.P. 2007 *Phys. Plasmas* **14** 102305
[35] Terry J.L. *et al* 2005 *Nucl. Fusion* **45** 1321
[36] Sattin F., Agostini M., Cavazzana R., Scarin P. and Terry J. 2009 *Plasma Phys. Control. Fusion* **51** 095004
[37] Xu X.Q., Nevins W.M., Rognlien T.D., Bulmer R.H.. Greenwald M., Mahdavi A., Pearlstein L.D. and Snyder P. 2003 *Phys. Plasmas* **10** 1773
[38] Bisai N., Das A., Deshpande S., Jha R., Kaw P., Sen A. and Singh R. 2005 *Phys. Plasmas* **12** 072520
[39] Bisai N., Das A., Deshpande S., Jha R., Kaw P., Sen A. and Singh R. 2005 *Phys. Plasmas* **12** 102515